AFRL-AFOSR-JP-TR-2024-0058

Anti-Static and Anti-flaming Improvement of Biodegradable Polymer Blends by Nanocoating via Plasma Technology and Sparking Process

CHONCHAROEN SAWANGRAT
SCIENCE AND TECHNOLOGY PARK, CHIANG MAI UNIVERSITY
155 MOO 2 MAE HIA
MUANG, , 50100
THA

03/07/2024
Final Technical Report

Air Force Research Laboratory
Air Force Office of Scientific Research
Asian Office of Aerospace Research and Development
Unit 45002, APO AP 96338-5002

REPORT DOCUMENTATION PAGE

PLEASE DO NOT RETURN YOUR FORM TO THE ABOVE ORGANIZATION.

1. REPORT DATE	2. REPORT TYPE	3. DATES COVERED	
20240307	Final	START DATE 20220926	END DATE 20230925

4. TITLE AND SUBTITLE
Anti-Static and Anti-flaming Improvement of Biodegradable Polymer Blends by Nanocoating via Plasma Technology and Sparking Process

5a. CONTRACT NUMBER	5b. GRANT NUMBER	5c. PROGRAM ELEMENT NUMBER
	FA2386-22-1-4064	61102F
5d. PROJECT NUMBER	**5e. TASK NUMBER**	**5f. WORK UNIT NUMBER**

6. AUTHOR(S)
Choncharoen Sawangrat, Kittisak Jantanasakulwong, Pornchai Rachtanapun, Jonghwan Suhr

7. PERFORMING ORGANIZATION NAME(S) AND ADDRESS(ES)
SCIENCE AND TECHNOLOGY PARK, CHIANG MAI UNIVERSITY
155 MOO 2 MAE HIA
MUANG 50100
THA

8. PERFORMING ORGANIZATION REPORT NUMBER

9. SPONSORING/MONITORING AGENCY NAME(S) AND ADDRESS(ES)	10. SPONSOR/MONITOR'S ACRONYM(S)	11. SPONSOR/MONITOR'S REPORT NUMBER(S)
AOARD UNIT 45002 APO AP 96338-5002	AFRL/AFOSR IOA	AFRL-AFOSR-JP-TR-2024-0058

12. DISTRIBUTION/AVAILABILITY STATEMENT
A Distribution Unlimited: PB Public Release

13. SUPPLEMENTARY NOTES

14. ABSTRACT
The research project emphasizes the widespread application of polymer blends, praising their exceptional attributes such as durability, lightweight, and chemical resistance, rendering them indispensable across diverse industries. As highlighted in a joint report from European Bioplastics and the nova-Institute, global bioplastics production surged to approximately 2.42 million tons in 2021. However, the use of biopolymers for packaging, electronics, and automotive applications is hindered by flammability and static. To address this, the project focuses on enhancing anti-flaming and antistatic packaging in electronic devices through plasma treatment and the introduction of nano-metal-particles (NMP).
In the project's initial phase, we successfully developed anti-flaming biodegradable composite films by melt blending PBS/PBAT, and epoxy with MgO. This resulted in PBS/E1/PBAT/MgO 15 blends achieving a V-1 degree of flame retardancy, with notable enhancements in tensile strength and elongation at break compared to PBS/PBAT. The improved properties stemmed from the epoxy reaction in the PBS/E1/PBAT blends, as confirmed by FTIR spectroscopy demonstrating the interaction between carboxyl groups of PBS and PBAT. Morphologically, the blends exhibited a well-distributed structure with MgO particles evenly dispersed in a PBS/E1/PBAT matrix. The addition of MgO improved thermal decomposition behavior and water resistance due to its high thermal stability and hydrophobicity. This reaction indicated improved compatibility, enhancing mechanical, water resistance, and thermal properties. MgO acted as a catalyst, making the anti-flaming biodegradable composite suitable for applications in packaging, medical, and agriculture. The upcoming phase will focus on preparing an anti-static and anti-flaming biodegradable composite film through nanocoating using plasma technology and sparking processes.

15. SUBJECT TERMS

16. SECURITY CLASSIFICATION OF:			17. LIMITATION OF ABSTRACT	18. NUMBER OF PAGES
a. REPORT U	b. ABSTRACT U	c. THIS PAGE U	SAR	43

19a. NAME OF RESPONSIBLE PERSON	19b. PHONE NUMBER *(Include area code)*
TODD RUSHING	315-227-7003

Standard Form 298 (Rev.5/2020)
Prescribed by ANSI Std. Z39.18

TABLE OF CONTENTS

TABLE OF CONTENTS (2)

TABLE OF FIGURES

TABLE OF TABLES

TABLE OF EQUATIONS

1. SUMMARY

The research project emphasizes the widespread application of polymer blends, praising their exceptional attributes such as durability, lightweight, and chemical resistance, rendering them indispensable across diverse industries. As highlighted in a joint report from European Bioplastics and the nova-Institute, global bioplastics production surged to approximately 2.42 million tons in 2021. However, the use of biopolymers for packaging, electronics, and automotive applications is hindered by flammability and static. To address this, the project focuses on enhancing anti-flaming and antistatic packaging in electronic devices through plasma treatment and the introduction of nano-metal-particles (NMP).

In the project's initial phase, we successfully developed anti-flaming biodegradable composite films by melt blending PBS/PBAT, and epoxy with MgO. This resulted in PBS/E1/PBAT/MgO 15 blends achieving a V-1 degree of flame retardancy, with notable enhancements in tensile strength and elongation at break compared to PBS/PBAT. The improved properties stemmed from the epoxy reaction in the PBS/E1/PBAT blends, as confirmed by FTIR spectroscopy demonstrating the interaction between carboxyl groups of PBS and PBAT. Morphologically, the blends exhibited a well-distributed structure with MgO particles evenly dispersed in a PBS/E1/PBAT matrix. The addition of MgO improved thermal decomposition behavior and water resistance due to its high thermal stability and hydrophobicity. This reaction indicated improved compatibility, enhancing mechanical, water resistance, and thermal properties. MgO acted as a catalyst, making the anti-flaming biodegradable composite suitable for applications in packaging, medical, and agriculture. The upcoming phase will focus on preparing an anti-static and anti-flaming biodegradable composite film through nanocoating using plasma technology and sparking processes.

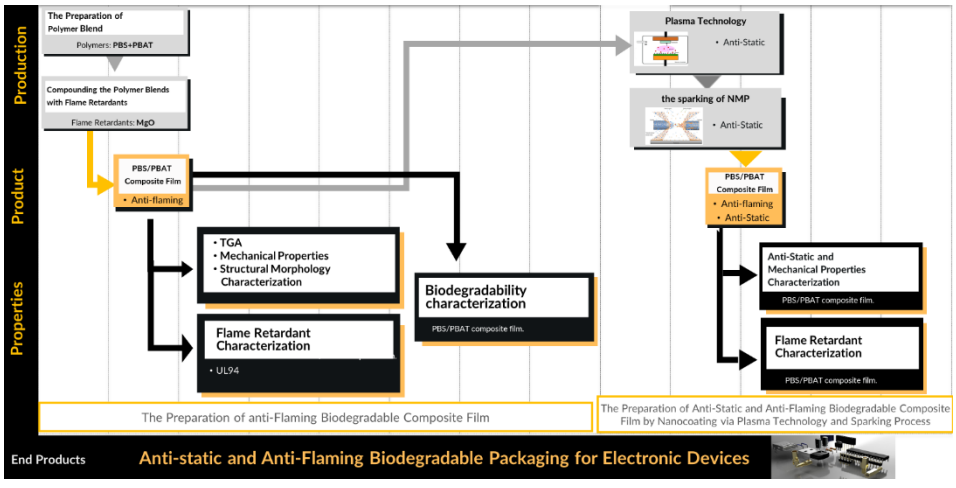

Figure 1. Research project process

2. INTRODUCTION

Since outstanding properties (e.g., durability, light-weight, corrosion resistance, chemical resistance, etc.), low-cost manufacturing, and easy processing of polymer blend, they are widely used in various industrial applications (Formela et al., 2018). Therefore, the world's plastic waste is growing each year. Only 9% of these wastes are successfully recycled while others end up in landfills, incinerators or leaking into environment (OECD, 2022). Additionally, the increase in plastic waste led to an environmental impact both on land and on marine life (Lee, 2018). The development of polymer blends is one way to solve this issue. There are three ways to classify these environmental-friendly materials including the origin of the polymer matrix (e.g., natural and synthetic polymers), degradability (e.g., fully, partially or non-biodegradable), and the content of renewable components (e.g., petroleum-based, partially or fully bio-based components) (Formela et al., 2018). According to the report from European Bioplastics in cooperation with the nova-Institute (Figure 2), global bioplastics production increased to approximately 2.42 million tons in 2021 which increase from 2020 to around 330 thousand tons. Therefore, the alternatives to new, cost-effective, and degradable plastic are currently a subject of interest for many academics and industries around the world.

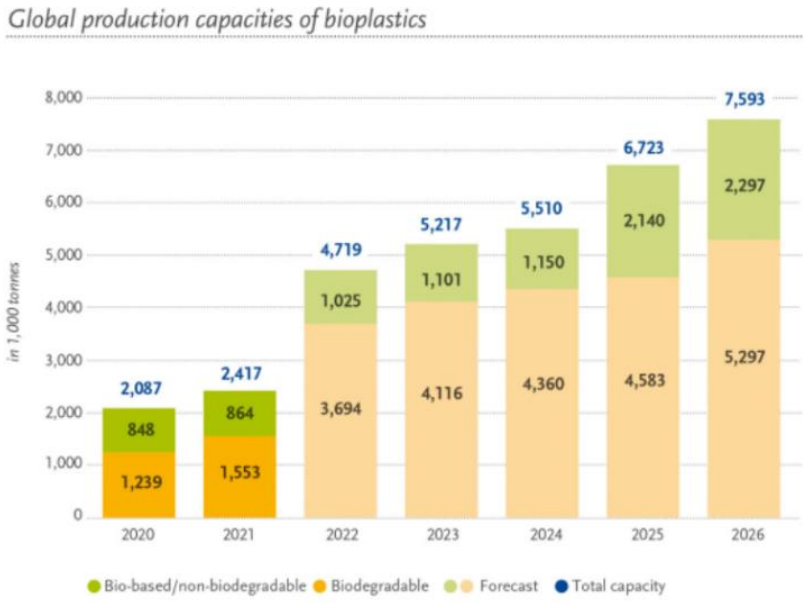

Figure 2. Global production capacities of bioplastics (European bioplastics, 2021)

Poly (Butylene succinate) (PBS) is one of the noticeable biodegradable polymers that can be generated by renewable resource-based succinic acid obtained by the bacterial fermentation of sugars, glucose, starch, xylose, etc. (Xu & Guo, 2010). Moreover, the melting

point for PBS (e.g., 115˚C) is considerably lower than other commercially available biodegradable polymers which could save industrial processing time for blending with other materials (Rafiqah et al., 2021). Other than that PBS is semi-crystalline nature, thermal stability, and ease of processing with conventional film casting and blowing techniques make it an appropriate representative for producing biodegradable films (de Matos Costa et al., 2020). However, the ductility of PBS is considerably poor and its price is high compared to other conventional plastics (Liminana et al., 2018). Therefore, there is still room to develop studies on PBS blends with other polymers. Poly (butylene adipate-co-terephthalate) (PBAT) is a synthetic polymer-based on fossil resources (Rodrigues et al., 2016) which is very ductile at room temperature and has good processability and hydrophilic properties (Deng et al., 2018). In this respect, PBAT is a suitable candidate for blending with PBS to achieve desirable physical, mechanical and barrier properties (de Matos Costa et al., 2020). A high potential for increasing material biodegradability can be achieved when blending PBAT and PBS (Bumbudsanpharoke et al., 2022). The expectation of blending the high ductility of PBAT and the tensile strength of PBS is to balance the properties of biodegradable film production (Nobile et al., 2018).

The limitation of using biopolymers in packaging, electronics, and automotive applications is the potential for fire risk or its flammability (Lule et al., 2021). Adding various types of flame retardants is a promising and effective way to improve the anti-flaming performance of a blending polymer matrix (Battegazzore et al., 2020; Feng et al., 2017; Jiang et al., 2018). However, Li et al. (2014) indicated that the efficiency and mechanism of MgO depend on the polymer matrix and there have been fewer studies. Moreover, an alternative flame retardant can be magnesium oxide (MgO) which has been widely used in the application of building materials, fireproof coatings, and refractory materials (Qin et al., 2019). Although MgO can be used as a binder in ceramics and ceramic-matrix (Stöckel et al., 2014), its use in polymer has not been investigated yet.

Atmospheric pressure plasma is an alternative technique for surface modification that will affect surface properties such as chemistry and morphology. Atmospheric pressure plasma has recently been demonstrated to be an effective technique for modifying polymer surfaces (Turkoglu Sasmazel et al., 2021). Only surface properties are charged, but the bulk properties remain unchanged when applying plasma treatment (Can-Herrera et al., 2016). Surface modification of polymer blends to increase surface area by plasma surface modification has been investigated to increase the adhesion of nanoparticles to the proposed composite material. Dhanumalayan et al. (2017) indicated that average surface roughness increased after plasma

treatment. Because static charges can destroy sensitive electronic equipment, researchers must develop antistatic materials (Al Ghufais et al.). The best candidate for the production of antistatic packaging is polymeric matrices due to their inherent lightness and good processability (Silva et al., 2019). Metal particles such as copper, silver, iron, etc. and carbon allotropes (carbon black, graphite or carbon nanomaterials) are commonly used for antistatic coating (Zoubek et al., 2019). Silva et al. (2019) indicated that electrically conductive particulate filers including metal or carbon nanoparticles can be added to electrically insulating polymeric matrices. However, there is still room to investigate an appropriately coated nanoparticle to improve the antistatic performance of composite polymers.

3. METHODS, ASSUMPTIONS AND PROCEDURES

3.1 The preparation of anti-flaming biodegradable composite film

3.1.1 The preparation of polymer blends and compounding with flame retardant

1) Preparation of biodegradable composites

The biodegradable composites were prepared using a melt-blending process. PBS was melt–blended with PBAT and epoxy at 0, 0.5, 1, 2, 5 and 10% using a two-roll mill (Figure 3.) at 130 ℃ for 10 min. The concentration of PBS, PBAT and epoxy are shown in Table 1. The melt blending of PBS/E/PBAT samples were mixed at this stage. The samples were compressed into sheets using hot compression molding at 130 ℃ for 10 mins. All samples were prepared into sheets to evaluate mechanical properties, and chemical structure characterization.

Figure 3. Images of two-roll mills melt mixing.

Table 1 Composition of PBS/E/PBAT blends.

Samples	Composition (wt/wt%)		
	PBS	E	PBAT
PBS	100	-	-
PBAT	-	-	100
PBS/PBAT	80	20	-
PBS/E0.5/PBAT	80	0.5	19.5
PBS/E1/PBAT	80	1	19
PBS/E2/PBAT	80	2	18
PBS/E5/PBAT	80	5	15
PBS/E10/PBAT	80	10	10

2) Preparation of anti-flaming biodegradable composite

Samples were prepared by melt-blending with the PBS mixed epoxy 1%, PBAT, and MgO at 0, 0.25, 0.5, 1, 2 and 5% using a two-roll mill at 130 ℃ for 10 min. Table 2 lists the compositions and nomenclature of the PBS/E1/PBAT/MgO blends. The samples were placed in a mold and compressed into sheets for properties assessments using a hot compress at 130 ℃ for 10 min.

Table 2 Composition of PBS/E1/PBAT/MgO blends.

Samples	Composition (wt/wt%)	
	PBS/E1/PBAT	MgO
1. PBS/E1/PBAT	100	-
2. PBS/E1/PBAT/MgO 0.5	99.5	0.5
3. PBS/E1/PBAT/MgO 1	99	1
4. PBS/E1/PBAT/MgO 2	98	2
5. PBS/E1/PBAT/MgO 5	95	5
6. PBS/E1/PBAT/MgO 10	90	10
7. PBS/E1/PBAT/MgO 15	85	15
8. PBS/E1/PBAT/MgO 12	80	20

3) Preparation of anti-flaming biodegradable composite blown film

The anti-flaming biodegradable composite was mixed using a twin-screw extruder (Figure 4.). Before mixing, all materials were dried at 60°C for 24 h to evaporate moisture content. The extruder temperatures of samples from the hopper to the die are 100–110–140–140–150–130–130–120 °C, corresponding to torque 50 and 70% and the speed of the screw is 80 rpm. After mixing the sample with a twin-screw extruder, the samples were produced films by extrusion blown film machine (Figure 5.). The temperature profile was set at 115–150–145–115–110°C from hopper to die, and the screw speed was set at 300 rpm. The film thickness was about 0.1–0.2 mm.

Figure 4. Images of twin-screw extruder for melt mixing

Figure 5. Images of extrusion blown film machine.

3.1.2 Mechanical properties and structural morphology characterization of PBS/E1/PBAT composite film.

1) Mechanical properties

The mechanical properties of PBS/E1/PBAT composite film were exhibited by tensile properties. The tensile properties of the samples were measured using a tensile tester (Model MCT–1150, Japan) at a distance of 10 mm and a crosshead speed of 20 mm/min. The specimens were prepared as bone-shaped samples according to the JIS K 6251–7 standard. A minimum of five specimens were tested for each composition. The specimens were conditioned at 25°C with 50 ± 2% RH for 24 h. The maximum force and elongation at break were recorded.

2) Water contact angles

Drop shape analysis of the sheets was performed using a drop shape analyzer (DSA30E, Krüss Co. Ltd., Hamburg, Germany). The samples were prepared as sheets measuring 20 mm × 20 mm × 1 mm (Width × Length × Thickness) and fixed on a glass slide. Water was dropped onto the surface of the sheets, and images were automatically recorded every minute for 10 min. After droplet formation, the water contact angle was measured by image analysis.

3) Morphological properties

The cross-sectional morphologies of films were examined by SEM (FE-SEM, JSM-IT800 series, JEOL Co., Ltd., Tokyo, Japan). The samples were prepared with dimensions of 5 mm × 30 mm × 1 mm (Width × Length × Thickness), placed in liquid nitrogen for 2 min, and broken to obtain cross-sectional fractured surfaces. All fractured sample surfaces were vacuum coated with a thin gold layer and observed at 15 kV. The morphology was characterized by the fracture surface of samples.

4) Chemical structure characterization by Fourier Transform Infrared Spectroscopy (FTIR)

The chemical structure characterization was investigated using FTIR spectroscopy (FT/IR–4700, Jasco Corp., Tokyo, Japan). The samples were prepared as films. The FTIR spectra were recorded between 4000 and 400 cm^{-1} with a resolution of 4 cm^{-1} 64 scans. The identification of chemical structure was obtained by the IR spectra analysis.

3.1.3 Flame retardant characterization with UL94, TGA and DSC

1) UL94 standard

The flame retardant of samples was tested by the UL94 standard (size: Widht 12.7 mm x Length 127 mm x Thickness 1 mm) for vertical burn (V-0 to V-2 Rating): A burner flame was applied to the free end of the specimen for two 10 second intervals separated by the time it takes for flaming combustion to cease after the first application. 5 specimens were tested. The classification of UL94 standards is shown in Table 3.

Table 3. Classification of UL94V standards

UL 94 Test (Vertical Burning Test)			
Test Criteria	V- 0	V- 1	V- 2
Burning time of each individual test specimens (s) (after first and second flame applications T_1 or T_2)	≤ 10 sec	≤ 30 sec	≤ 30 sec
Total burning time (S) (T_1+T_2)	≤ 50 sec	≤ 250 sec	≤ 250 sec
Dripping of burning specimen (ignition of cotton batting)	No	No	Yes
Combustion up to holding clamp (specimens completely burned)	No	No	No

2) Thermogravimetric analysis (TGA)

Thermogravimetric analysis (TGA) of all samples was observed using the thermogravimetric analyzer. TGA was performed under N_2 using a thermogravimetric analyzer (Mettler–Toledo STARe system TGA/DSC3+, Greifensee, Switzerland), with each sample weighing approximately 5 – 10 mg. The samples were heated from 25 to 600°C at a heating rate of 15°C/min.

3) Differential Scanning Calorimetry (DSC)

The samples 5 – 10 mg were placed in alumina pans. The program was employed according to the temperature: heating from −50 to 200°C, cooling from 200 to −50°C, further heating from −50 to 200°C, with a constant heating rate of 10°C/min and under a nitrogen atmosphere. The crystallinity (%X_c) of samples was calculated using Equation (1)

$$\%\mathrm{Xc} = \left(\frac{\Delta H_m - \Delta H_c}{\omega H_0^m}\right) \times 100 \qquad (1)$$

where ΔH_m and ΔH_c are the enthalpies of melting and cold crystallization, respectively, and ω and ΔH^0_m are the weight fraction of PBS and PBAT and the melting enthalpy of 100% (110 and 114 J/g), respectively.

3.1.4 Statistical analysis

Analyze the results used with One-way ANOVA with SPSS software. The statistically analyzed result was used in tensile strength and water contact angle. The differences found ($P < 0.05$) were estimated using the Duncan's test.

3.2 The preparation of anti-static and anti-flaming biodegradable composite film by nanocoating via plasma technology and sparking process.

3.2.1 The use of plasma treatment and the sparking of nano-metal-particles (NMP) on PBS/E1/PBAT/MgO composite film.

1) Plasma treatment

The PBS/E1/PBAT/MgO composite film were functionalized using copper (Cu), zinc (Zn), aluminum (Al), and titanium oxide (TiO_2) nanoparticles through DC magnetron sputter coating employing the magnetron sputtering system (MSLV-20020330) (Figure 6.). The procedure for depositing nanoparticles on the PBS/E1/PBAT/MgO composite film was as follows:

A high-purity (99.99%) target was secured on the cathode end within a 5 mm distance from the specimen's surface. The vessel was evacuated before sputtering by insertion of gas. The argon (Ar) gas pressure was maintained at 1.0×10^{-1} Torr/m^3 in the chamber, and the Ar gas was stabilized through panel control. The oxygen (O_2) gas pressure was set at 3.0 x 10-1 Torr/m^3, with a constant flow of 5 sccm. The substrate underwent a smooth deposition of metal nanoparticles using DC magnetron sputter coating, powered by a 100 W DC power supply (RPG-50 reactive plasma generator) for the sputtering process (Figure 7.). The coating duration was set to 3 mins, and the coating processes were applied to only one side of the PBS/E1/PBAT/MgO composite film. Following the sputter coating, the final nanocomposite of PBS/E1/PBAT/MgO composite film was extracted from the chamber for the measurement of its physical, chemical, and electrical characteristics.

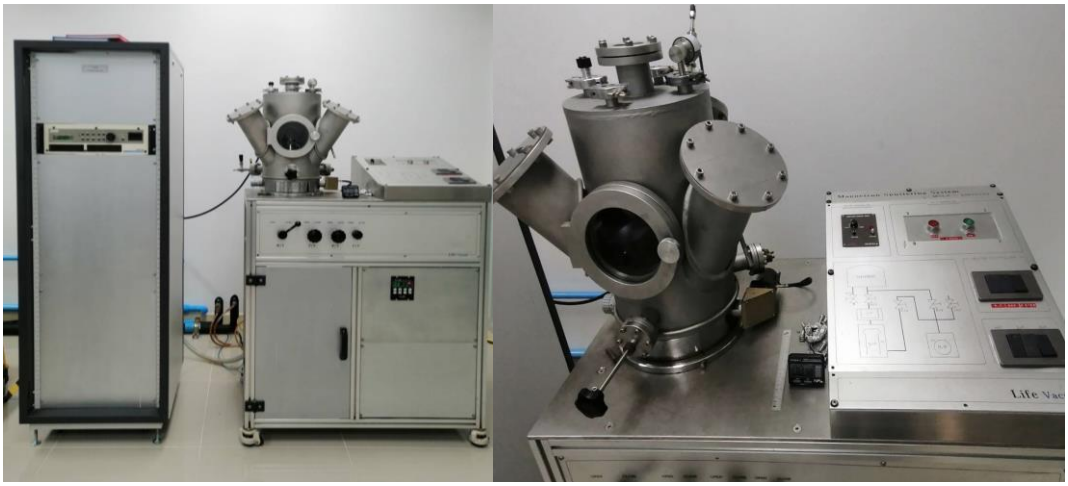

Figure 6. Image of direct current DC magnetron sputter machine

Figure7. The process of the formation of nanoparticles over the surface of PBS/E1/PBAT/MgO composite film by DC magnetron sputter coating method.

2) Sparking Process

The Ti, Cu, and Al wires (0.5 mm diameter) were purchased from Advent Research Materials Co., Ltd. (Oxford, UK). The two sharp tips (20 mm length) of metal wire were connected with the anode and cathode of a sparking machine (Figure 8.). The tips were aligned at 2 mm above the PBS/E1/PBAT/MgO composite film (Width x Length x Thickness 5 x 10 x 0.1 cm) with a 1 mm gap between the anode and cathode. PBS/E1/PBAT/MgO composite film was sparked at 3 kV and 3 mA, and the tip holders of the wires were moved along the XY axes at a speed of 100 mm/min.

Table 4. Conditions of sparking process of PBS/E1/PBAT/MgO composite film

No.	Metal wire: Repeated times
1	Control (Untreated)
2	Titanium (Ti: 10)
3	Titanium (Ti: 20)
4	Titanium (Ti: 30)
5	Titanium (Ti: 40)
6	Copper (Cu: 40)
7	Aluminium (Al: 40)

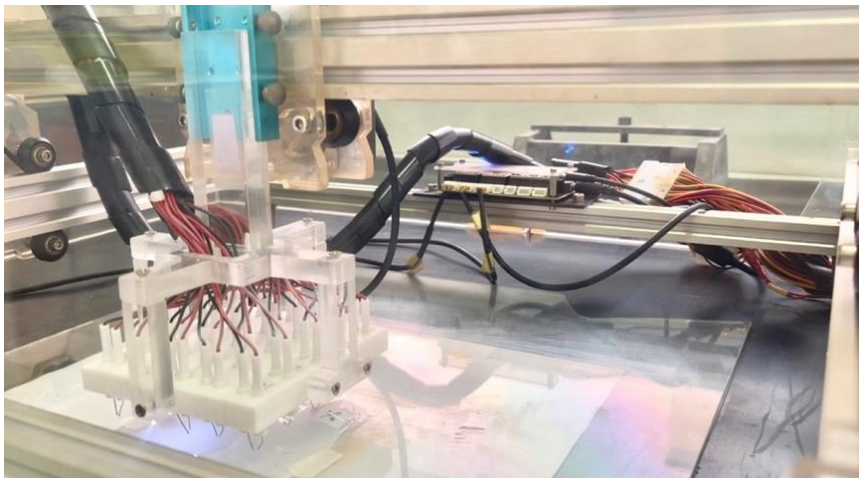

Figure 8. The apparatus used for deposited PBS films with metals oxide nanoparticles by sparking machine.

3.2.2 Biodegradability characterization of PBS/E1/PBAT/MgO composite film.

The test was carried out in flasks to provide gas exchange between the inner atmosphere and the outside environment according to ISO 20200. The composition of the synthetic waste used in this method is described in Table 1. In each flask, 500 g of synthetic compost was mixed with de-ionized water to the mixture to adjust its final water content to 55 % in total. The sample and placed on the bottom, forming a homogeneous layer. The test was conducted in thermophilic incubation conditions at 58 ± 2 °C.

Table 5. Composition of synthetic solid waste

Materials	**Dry mass (%)**
Sawdust	40
Rabbit-feed	30
Ripe compost	10
Corn starch	10
Saccharose	5
Corn seed oil	4
Urea	1
Total	**100**

4. RESULTS AND DISCUSSION

4.1 The preparation of anti-flaming biodegradable composite film

4.1.1 The preparation of polymer blends (PBS/PBAT) and compounding with flame retardant (MgO)

1) Mechanical properties of PBS/E1/PBAT composite film

Figure 9. presents the tensile properties of PBS, PBAT, PBS/PBAT, and PBS blend with epoxy at 0.5– 10% and PBAT. PBS was melt-blended with 0.5– 10% epoxy and PBAT. The tensile strength of the PBS, PBAT, PBS/PBAT, and PBS blended with epoxy at 0.5, 1, 2, 5, and 10 and PBAT were 24.9, 20.9, 19.0, 20.4, 25.3, 17.3, 18.9, 18.2 and 18.2 MPa, respectively. The combination of PBS and PBAT resulted in a decrease in elongation at the break compared to pure PBS and PBAT. The addition of epoxy at 1% resulted in the highest tensile strength but decreased in elongation at break. This indicated the crosslinking of PBS or PBAT through a reaction with epoxy resin. The tensile property reduction of PBS blends with epoxy at 2–10% and PBAT indicated an excessive amount of epoxy, which increased incompatibility between PBS and PBAT. The PBS/E1/PBAT sample is the best formulation for producing this biodegradable composite film.

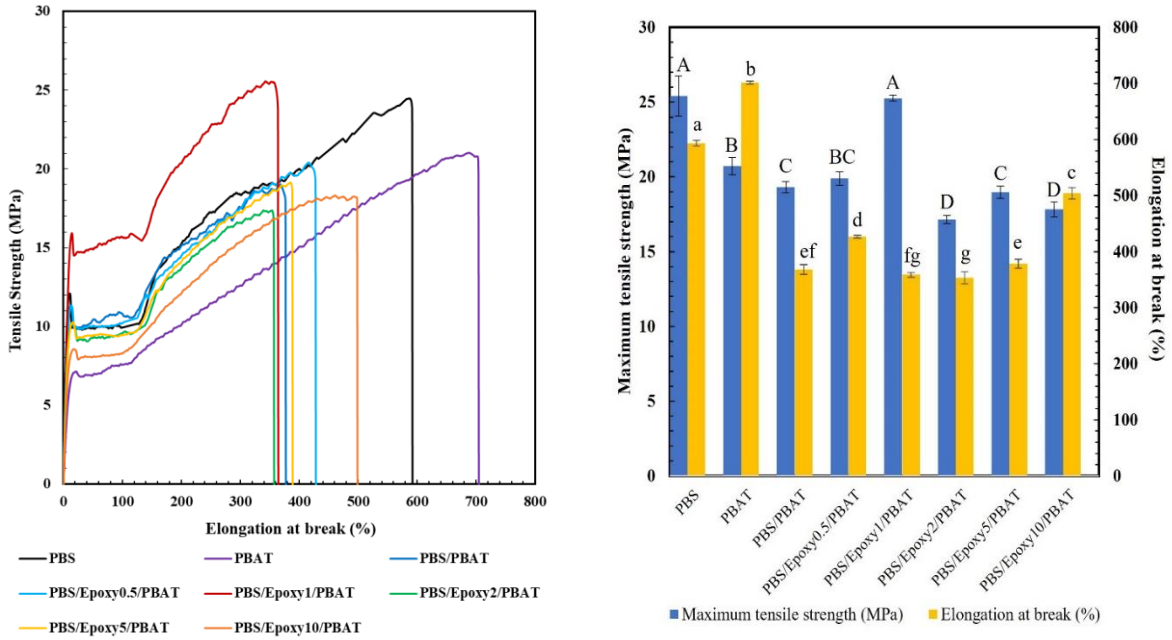

Figure 9. Tensile properties of PBS, PBAT, PBS/PBAT, PBS blend with epoxy at 0.5, 1, 2, 5, and 10% and PBAT. The mean values of the elongation at break (Lowercase letters) and maximum tensile strength (Uppercase letters) differ significantly ($P < 0.05$)

2) Chemical structure characterization of PBS/E1/PBAT composite film

The chemical structure was observed using FTIR spectroscopy. The FTIR spectra of Epoxy, PBS, PBAT, PBS/PBAT, and PBS blend with epoxy at 0.5 – 10% and PBAT are shown in Figure 10. The FTIR spectra of epoxy showed peaks of C=C stretching bands of aromatic rings (914 and 1670 cm^{-1}), and C–C stretching of the aromatic ring (1455, 1508, 1581, and 1606 cm^{-1}). PBS presented characteristic peaks at 918 cm^{-1}(–C–OH bending), 1045 cm^{-1}(–O–C–C– stretching), 1153 cm^{-1}(–C–O–C– stretching), 1713 cm^{-1} (C=O stretching) and 1332 and 2944 cm^{-1} (–CH_2– groups), respectively. The FTIR spectra of PBAT showed peaks at 726, 1249, and 1710 cm^{-1} corresponding to the –CH_2– stretching of the polymer backbone, stretching of the C–O groups from ester bonds, and C=O in the ester linkage, respectively. The PBS/PBAT and PBS with epoxy 0.5 – 10% and PBAT blends showed combination spectra of PBS, PBAT, and epoxy for each formula. In the PBS/E1/PBAT blend, the intensity of the peak at 1249 cm^{-1} of C–O stretching groups decreased indicating a change in the C–O vibration due to the reaction between the carboxyl end groups of PBS and PBAT with epoxy.

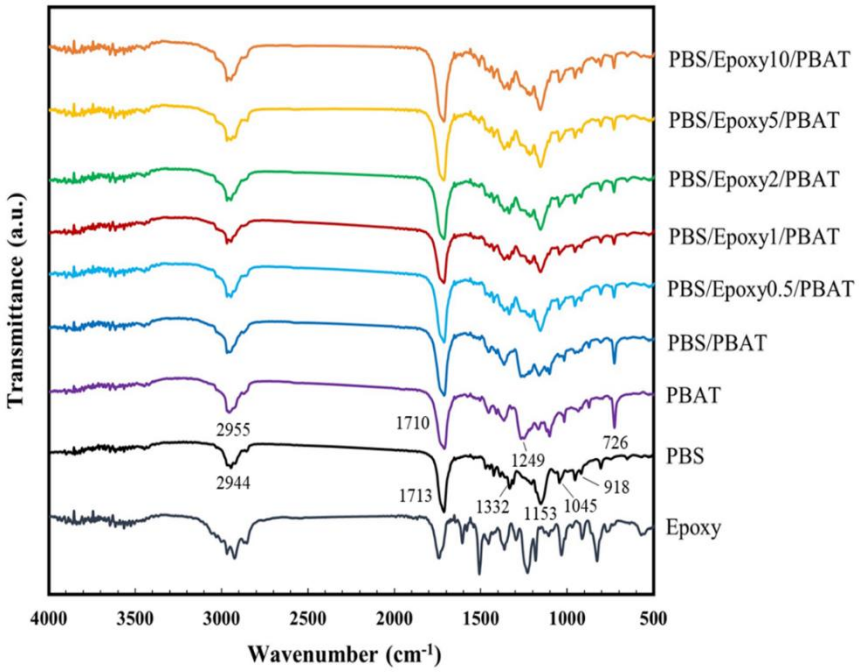

Figure 10. FTIR spectra of epoxy, PBS, PBAT, PBS/PBAT, and PBS with epoxy 0.5 – 10% and PBAT blends at 500–4000 cm^{-1}

3) UL94 standard testing of PBS/E1/PBAT/MgO composite film

The UL94 standard Vertical Burning test was used to determine the flammability of the samples. The UL–94 ratings classification flammability of PBS, PBAT, PBS/PBAT, and PBS/E 0.5 – 20/PBAT samples are represented in Table 6. The PBS, PBAT, PBS/PBAT, and PBS/E1/PBAT exhibited a V-2 flame retardancy rating which the flaming drips were observed after the samples burned but were not burned up to the holding clamp (Figure 11a.). The addition of 0.5 – 2% MgO in PBS/E1/PBAT extended the burning time to over 30s and 60s for T_1, and 250s for T_1+T_2. The addition of MgO at 5, and 15% showed a continuous improvement in flammability with T_1 at 12s, 12s, and 14s and T_1+T_2 at 128s, 125s, and 122s. Particularly, The PBS/E1/PBAT/MgO 15 represents a V-1 degree of flame retardancy because the drips of samples were not ignited cotton batting (Figure 11b.). These results indicated the flame-retardant properties of MgO.

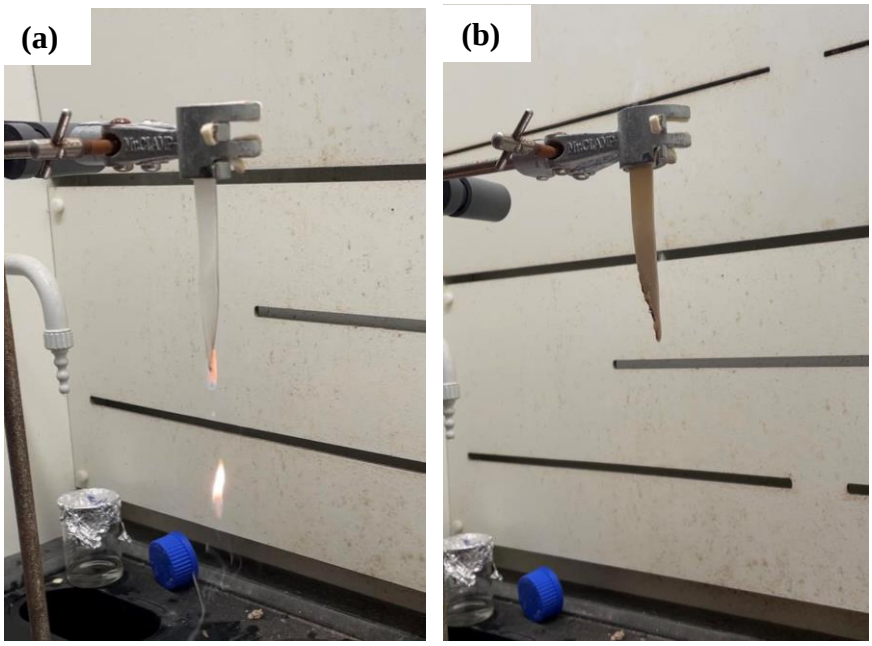

Figure 11. Image of drip samples (a) flaming drip (b) non–flaming drip.

Table 6. Anti-flame ability of PBS, PBAT, PBS/PBAT, and PBS blend with epoxy at 0.5 – 10% and PBAT.

Samples	Class UL 94 (V0-V2)	T_1 (s)	$T_1 + T_2$ (s)	Ignition (flaming drip) (Yes/No)	Specimen burns up to holding clamp. (Yes/No)
PBS	V-2	1	10	Yes	No
PBAT	V-2	1	10	Yes	No
PBS/PBAT	V-2	1	0	Yes	No
PBS/E1/PBAT	V-2	2	14	Yes	No
PBS/E1/PBAT/MgO 0.5	-	over 60	over 250	Yes	No
PBS/E1/PBAT/MgO 1	-	over 30	over 250	Yes	No
PBS/E1/PBAT/MgO 2	-	over 30	over 250	Yes	No
PBS/E1/PBAT/MgO 5	V-2	12	128	Yes	No
PBS/E1/PBAT/MgO 10	V-2	12	125	Yes	No
PBS/E1/PBAT/MgO 15	V-1	14	122	No	No

4) Mechanical properties of PBS/E1/PBAT/MgO composite film

The tensile properties of PBS, PBAT, PBS/PBAT, PBS/E1/PBAT, and PBS/E1/PBAT/MgO at 0.5 – 15% are presented in Figure 12. The tensile strength of PBS (25 MPa) was higher than that of PBAT (20 MPa). However, the elongation at break of PBS (593 %) was lower than that of PBAT (701%). The PBS/PBAT blend showed tensile strength and elongation at break of 19 MPa and 367%, respectively. Upon adding Epoxy 1% to PBS/PBAT, the tensile strength increased to 25 MPa, and the elongation at break decreased to 358% owing to increasing of compatibility between PBS and PBAT by epoxy reaction. The addition of 0.5 – 15% MgO to PBS/E1/PBAT reduced the tensile strength compared to the PBS/E1/PBAT blend. PBS/E1/PBAT/MgO 0.5 exhibited the highest tensile strength of 22 MPa. The addition of 1-5% MgO in PBS/E1/PBAT resulted in decreased tensile strength and elongation at the break due to the presence of agglomerates and large particles, which reduced compatibility between PBS/E1/PBAT and MgO. However, the elongation at break of PBS/E1/PBAT/MgO 10 – 15% was increased to 415.9 and 505.2% due to the higher quantity and better dispersion of MgO in the matrix.

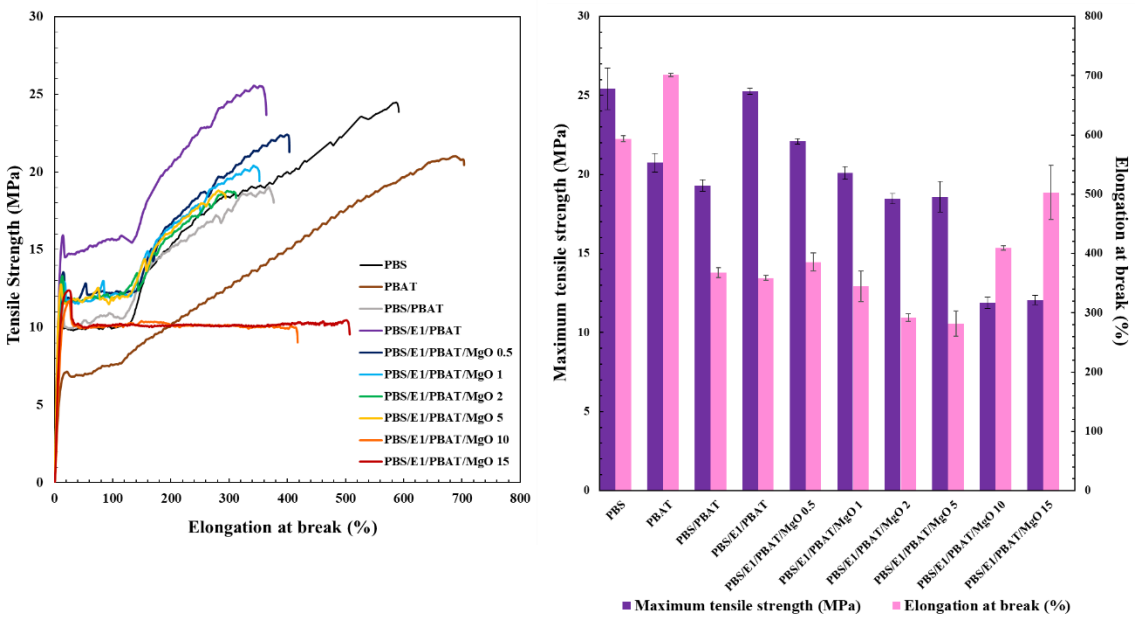

Figure 12. Tensile properties of PBS, PBAT, PBS/PBAT, PBS/E1/PBAT, and PBS/E1/PBAT blend with 0.5–15% MgO. Mean values of the elongation at break (lowercase letters) and maximum tensile strength (uppercase letters) differ significantly ($p < 0.05$).

5) Thermogravimetric analysis (TGA) of PBS/E1/PBAT/MgO composite film

Figure 13. presents the TGA thermograms of PBS, PBAT, PBS/PBAT, PBS/E1/PBAT, and PBS/E1/PBAT/MgO 0.5 – 15%. The PBS, PBAT, PBS/PBAT, and PBS/E1/PBAT showed one main weight loss stage and heat flow peak. The weight loss stage of PBS and PBAT were 409 and 413°C, respectively, which were the main thermal degradation of the polymers. The PBS/PBAT had the weight loss stage at around 409°C, while the weight loss stage of PBS/E1/PBAT slightly increased to 410°C indicating the crosslinking of PBS, PBAT, and epoxy. In the TGA thermogram of the PBS/E1/PBAT/MgO 0.5 – 15%, main step weight loss appeared in the range of 398–400°C, which related to depolymerized polymer under the catalysis of MgO. However, the addition of MgO at 2 – 15% showed a multiple-stage weight loss, including two stages for PBS/E1/PBAT/MgO 2 and 5%, with the first stage at 310–320°C and the second at 395–400°C. The weight loss stage at 310–320°C indicated the de-hydroxylation of the MgO particles' surface in polymer composites. For PBS/E1/PBAT/MgO 10 – 20%, there were three stages with the first at 310–320°C, the second at 390–400°C, and the third at 450–460°C (Heat transfer of MgO in polymer blend). In addition, the %residue at 600°C of the PBS/E1/PBAT/MgO 10, and 15% were obtained to be 19% and 23%, respectively. The increasing %residue could be related to the presence of inorganic MgO particles and its high thermal stability.

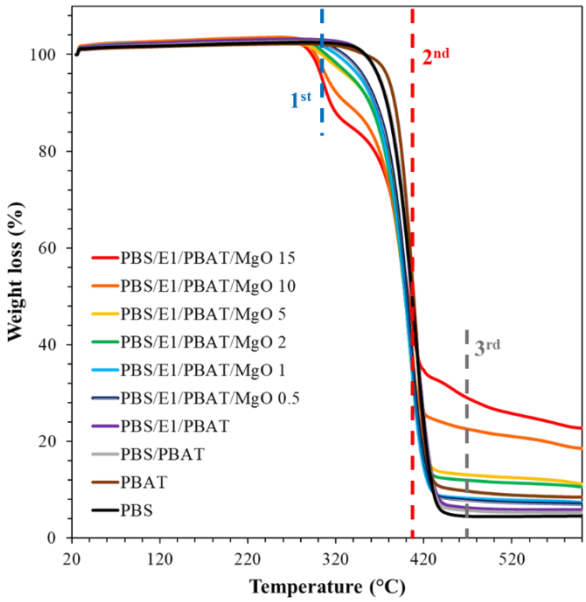

Figure 13. TGA thermograms of PBS, PBAT, PBS/PBAT, PBS/E1/PBAT, and PBS/E1/PBAT/MgO 0.5 – 15%.

6) Differential scanning calorimetry (DSC) of PBS/E1/PBAT/MgO composite film

DSC curves are used to determine the thermal properties of the PBS/E1/PBAT/MgO blend. Figure 14 shows the second scan of DSC curves of PBS, PBAT, PBS/PBAT, PBS/E1/PBAT, and PBS/E1/PBAT/MgO15. The PBAT exhibited T_g (Glass transition temperature) values of -28°C, and Tm (Melting temperature) was 121°C. The T_m of PBS was 87°C, while the Tg was not observed (Table 7). The Tm of PBS/PBAT, PBS/E1/PBAT, and PBS/E1/PBAT/MgO 15 were presented at 87, 87 and 86°C, respectively. The PBS/PBAT, PBS/E1/PBAT, and PBS/E1/PBAT/MgO15 blends showed a decrease in T_m compared with PBS because of the formation of small crystal size of PBS. The crystallinity of PBS, PBAT, PBS/PBAT, PBS/E1/PBAT, and PBS/E1/PBAT/MgO 15 were 43, 11, 26, 29, and 19%, respectively. However, recrystallization was not observed in all the blends due to the high crystal content without a nucleation crystal to induce the new crystallization.

Table 7. Second scan DSC results of PBS, PBAT, PBS/PBAT, PBS/E1/PBAT, and PBS/E1/PBAT/MgO 15.

Sample	**T_g (°C)**	**T_c (°C)**	**T_m (°C)**	**ΔH_m (J/g)**	**ΔH_c (J/g)**	**ΔX_c (%)**
PBS	-	-	87.50	47.12	-	42.83
PBAT	-28.20	-	121.50	12.93	-	11.34
PBS/PBAT	-	-	87.10	33.90	-	26.35
PBS/E1/PBAT	-	-	87.10	31.43	-	28.57
PBS/E1/PBAT/MgO15	-	-	86.80	21.05	-	19.13

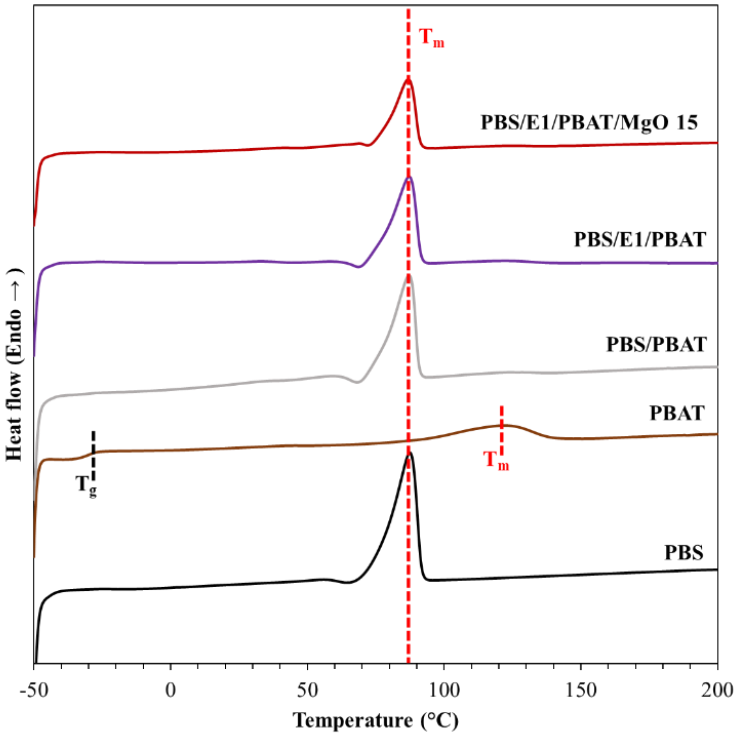

Figure 14. DSC curves of the second scan of PBS, PBAT, PBS/PBAT, PBS/E1/PBAT, and PBS/E1/PBAT/MgO15.

7) Water contact angles of PBS/E1/PBAT/MgO composite film

The water contact angles of the PBS, PBAT, PBS/PBAT, PBS/E1/PBAT, and PBS/E1/PBAT/MgO at 0.5–15% are shown in Figure 15. The water droplet was absorbed into the surface, and the contact angle was automatically recorded every 1 min for 10 min. PBS had a contact angle of 77.8° after 10 minutes, while PBAT had a higher angle at 82.7°. PBS exhibited higher hydrophilicity than PBAT. The PBS/PBAT blend had a contact angle of 80.7° and the contact angle was higher than PBS. The addition of Epoxy 1% to PBS/PBAT increased the contact angle to 80.9° because of the compatibility of the blend. In the PBS/E1/PBAT blend with 0.5% and 1% MgO, the water contact angle at 10 minutes increased to 83.0° and 85.7°, respectively. The results indicated that the addition of MgO 1% to the PBS/E1/PBAT increased the surface tension of the PBS/E1/PBAT blend, owing to the hydrophobicity of the metal particles. Nevertheless, Adding MgO at 2, 5, 10, and 15% decreased water contact angles (10min) to 75.0°, 72.9°, 65.8°, and 63.6°, respectively, due to increasing of roughness of the composite films' surfaces and alkaline MgO whiskers.

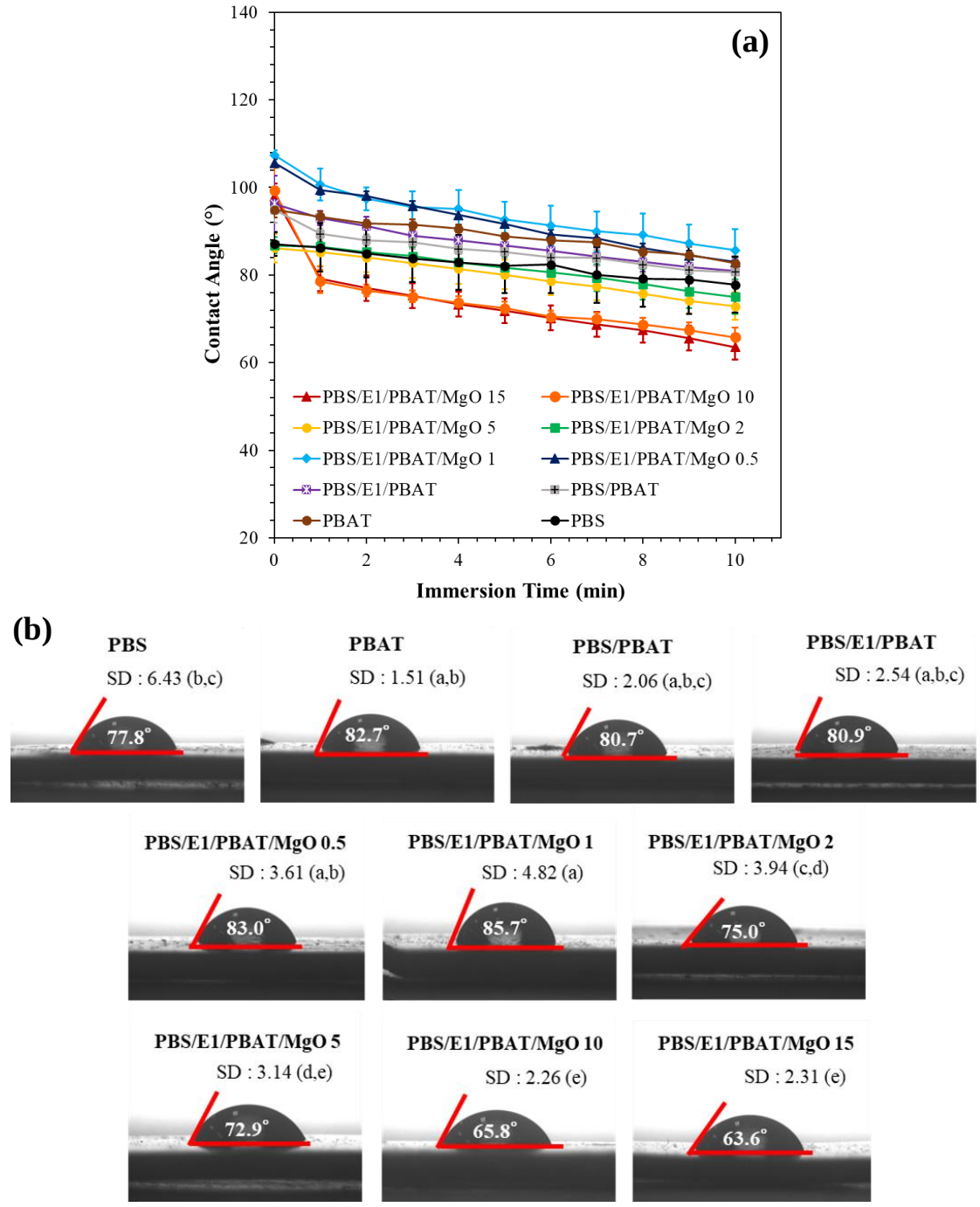

Figure 15. Water contact angles of PBS, PBAT, PBS/PBAT, PBS/E1/PBAT and PBS/E1/PBAT/MgO 0.5–15% (a) plots of samples and (b) values at 10 min.

8) Morphology of PBS/E1/PBAT/MgO composite film

Figure 16 shows the SEM images of the fracture surfaces of PBS, PBAT, PBS/PBAT, PBS/E1/PBAT and PBS/E1/PBAT with 0.25–5% MgO blends. PBAT showed a smooth fracture surface image while PBS lightly presented a rough fracture surface. The PBS/PBAT blend exhibited an increase in the rough fracture surface because of the incompatibility of the phase between PBS and PBAT. The PBS/PBAT blend exhibited an increase in the rough fracture surface because of the incompatibility of the phase between PBS and PBAT. Meanwhile, the PBS/E1/PBAT showed a rise in the smooth fracture surface and dispersion of epoxy around materials because epoxy improved the compatibility of the PBS/PBAT blend. In the addition of MgO at 0.5–5 in PBS/E1/PBAT blends, the rough fracture surface of the blends increased with MgO content due to agglomeration of MgO particles in the samples. However, addition MgO 10 and 15% showed the smoother surface due to the well-dispersed MgO, which increased elongation at break of PBS/E1/PBAT/MgO 10 and 15%.

Figure 17 shows the SEM-EDS of MgO on the fracture surfaces of PBS/E1/PBAT with 0.5–20% MgO blends. In the SEM-EDS image, the PBS/E1/PBAT with 0.5–5% MgO blends were agglomerated on the matrix and increased the large MgO particles. The poor distribution of MgO particles in the PBS/E1/PBAT resulted in a decrease in the mechanical properties of the blends. The addition of MgO at 10–15 showed increasing dispersion in the matrix indicating the improvement of elongation at the break of the blends.

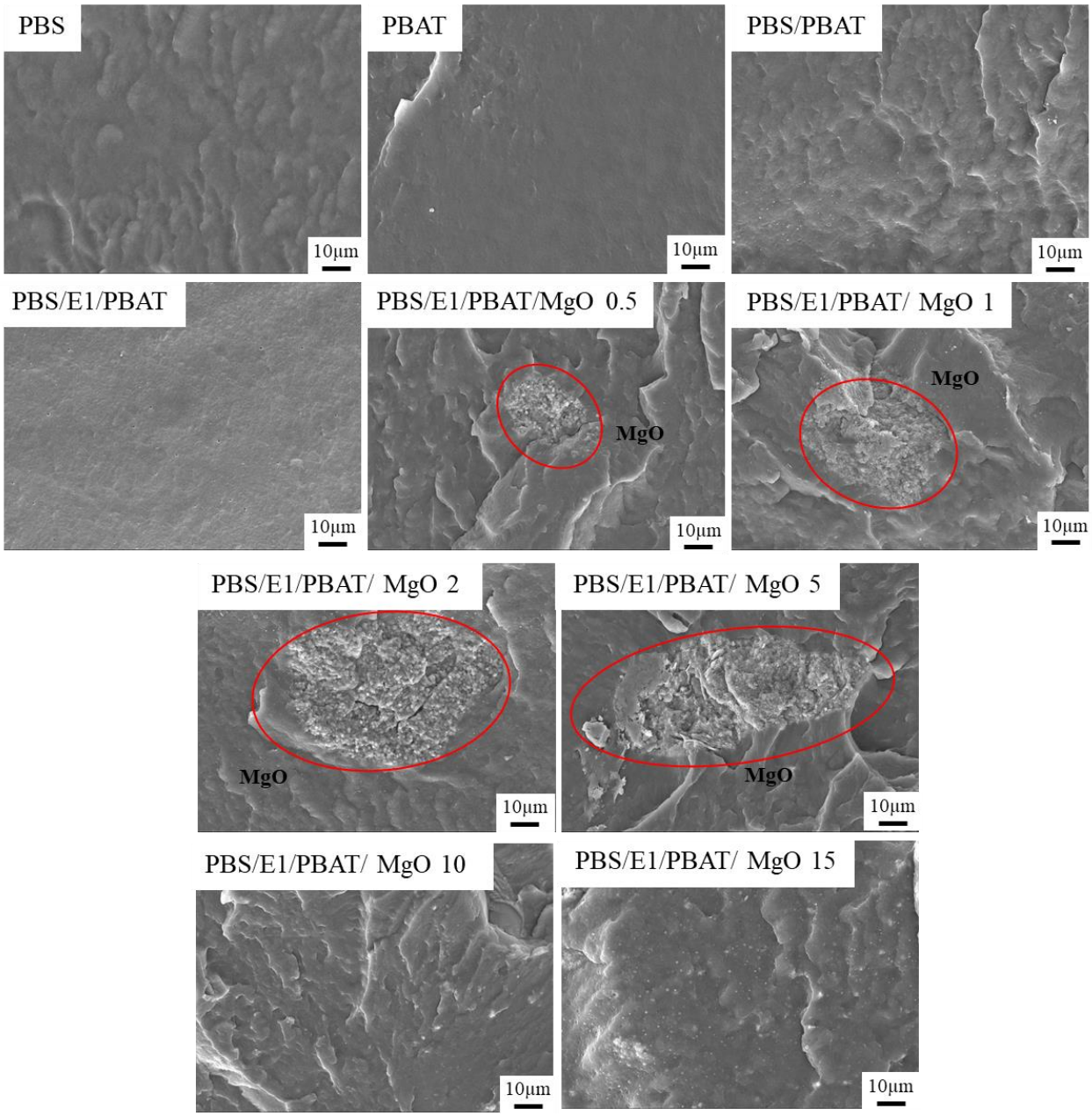

Figure 16. Scanning electron micrographs of PBS, PBAT, PBS/PBAT, PBS/E1/PBAT and PBS/E1/PBAT/MgO 0.5–15%.

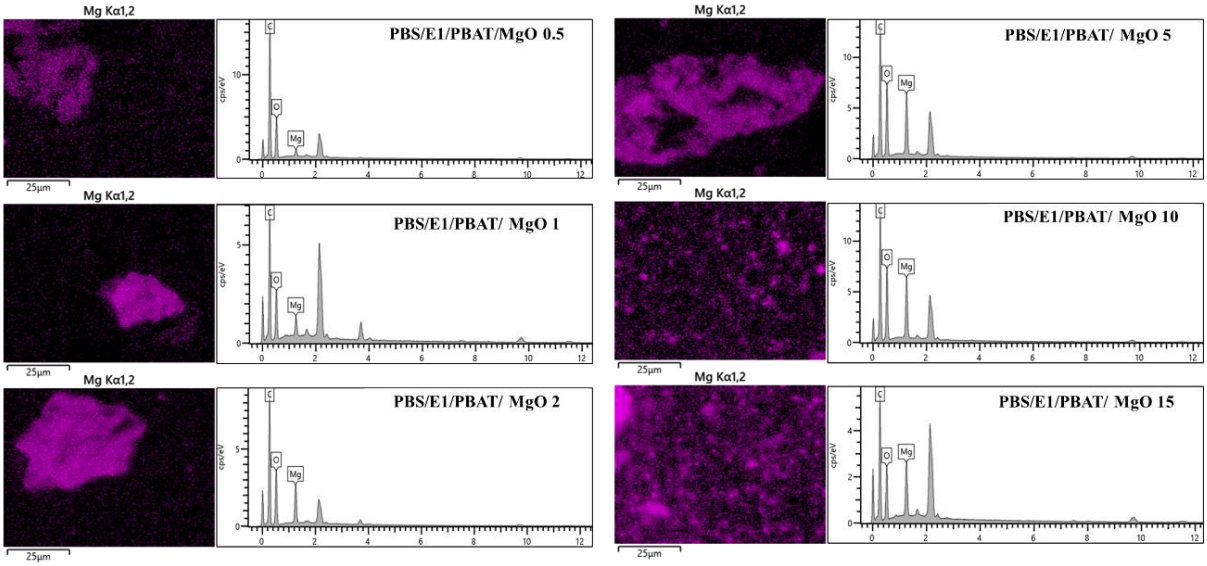

Figure 17. EDS mode of PBS/E1/PBAT/MgO 0.5–15%.

9) Chemical structure of PBS/E1/PBAT/MgO composite film

Figure 18 presents the FTIR spectra of PBS, PBAT, PBS/PBAT, PBS/E1/PBAT, and PBS/E1/PBAT/MgO at 0.5 – 15%. The chemical structure of the blends was studied by FTIR spectroscopies. The epoxy showed characteristic peaks at 914 and 1670 cm^{-1} due to epoxy groups' absorption and C=C stretching bands of aromatic rings, respectively. The peaks at 1455, 1508, 1581, and 1606 cm^{-1} corresponded to the C–C stretching vibration of the aromatic ring. The peak of PBS at 918 cm^{-1} corresponds to the –C–OH bending in the carboxylic acid groups. The bands at 1045 cm^{-1} was due to –O–C–C– stretching vibrations in PBS. Peaks in the range of 1153 cm^{-1} resulted from the stretching of the –C–O–C– group in the ester linkages of PBS. The band at the 1713 cm^{-1} region was attributed to the C=O stretching vibrations of ester groups. Meanwhile, the peaks at 1332 and 2944 cm^{-1} were assigned to the symmetric and asymmetric deformational vibrations of $–CH_2–$ groups in the PBS main chains, respectively. PBAT showed a peak at 726 cm^{-1}, which was associated with the vibrations of $–CH_2–$ adjacent methylene groups of the polymer backbone. A peak in the region of 1249 cm^{-1} was assigned to the stretching of the C–O groups from ester bonds. The most intense of all the peaks appears in the region of 1710 cm^{-1} and was attributed to the carbonyl groups (C=O) in the ester linkage. MgO showed peaks at 409 and 666 cm^{-1}, which indicated the vibrations of Mg–O of the MgO particles. The bands at 1418 cm^{-1} was due to C=C stretching vibrations in MgO. A peak in the region of 3367 cm^{-1} is assigned to the OH groups in MgO particles. The PBS/E1/PBAT with 0.5 – 15% MgO exhibited combined characteristics of PBS, PBAT,

Epoxy, and MgO spectra. The FTIR spectra of the PBS/E1/PBAT/MgO blends exhibited the combination spectra. In PBS/E1/PBAT/MgO0.5, two peaks about 1246 cm^{-1} were observed while one of peak decreased with MgO content due to MgO acting as a catalyst for –COOH and epoxy reaction.

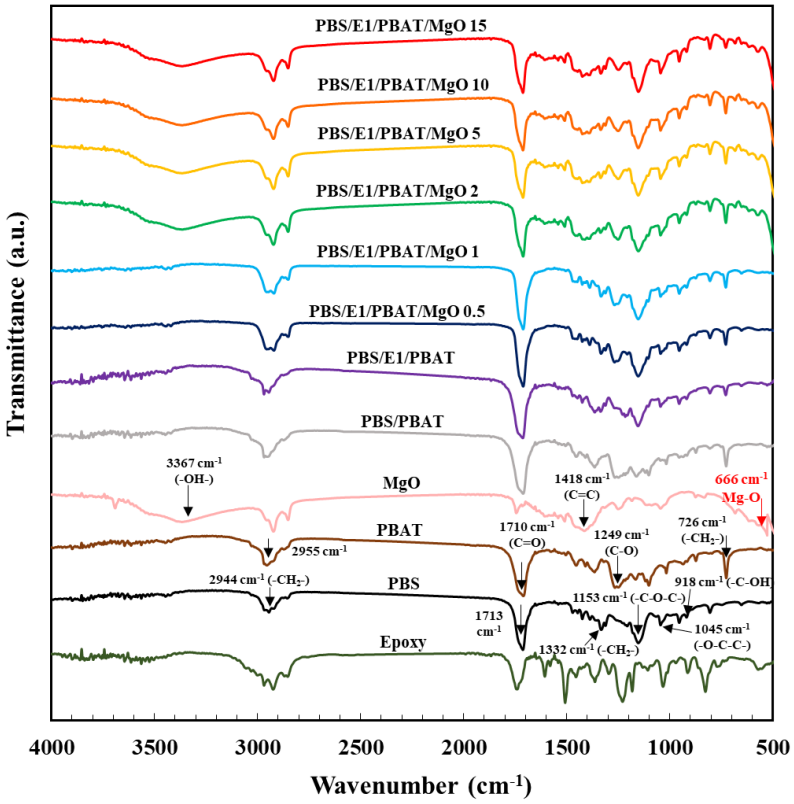

Figure 18. FTIR spectra of PBS, PBAT, PBS/PBAT, PBS/E1/PBAT and PBS/E1/PBAT/MgO 0.5–15%.

4.2 The preparation of anti-static and anti-flaming biodegradable composite film by nanocoating via plasma technology and sparking process.

4.2.1 The use of plasma treatment and the sparking of nano-metal-particles (NMP) on PBS/E1/PBAT/MgO composite film.

Fig 19 shows the anti-static property of the PBS/E1/PBAT/MgO composite coated with Ti, Cu, Al, and Zn using magnetron plasma sputter and spark methods. Nanolayer films of TiO_2, Cu_2O, Al_2O_3, and ZnO were deposited on the surface of the PBS/E1/PBAT/MgO composite. These metal oxide thin films enhance the electronic conductivity of the samples.

Plasma sputter treatment significantly improved the anti-static properties of the PBS/E1/PBAT/MgO composite compared to the control. Table 8 summarizes the average static electricity values of the PBS/E1/PBAT/MgO composite, with each datum representing

the mean of five measurements. It was found that the PBS/E1/PBAT/MgO composite coated with a metal oxide film exhibited lower static electricity values than the control. It is worth noting that the lower the charge density, the better the anti-static property of the sample (Chongqi et al., 2010). Notably, better anti-static behavior was observed when the sputter treatment had a low discharge power, while the spark treatment showed better results when treated for a shorter period of time. Unlike sputtering, spark treatment did not significantly improve the anti-static properties of the PBS/E1/PBAT/MgO composite compared to the control.

Using the plasma sputter technique to coat the PBS/E1/PBAT/MgO composite with metal or metal oxide resulted in better anti-static properties than the spark method. Magnetron sputter deposition is a vacuum technique that applies high power via low-pressure gas to form active gas particles. During the coating process, these gas particles interact with the object and cause the transfer of atoms from the object to the materials. As a result, magnetron sputter coating offers advantages such as controlling the thickness of the nanolayer film, high speed, proper adhesion, high purity, and stability (Linss, 2017; Mohamed et al., 2021)

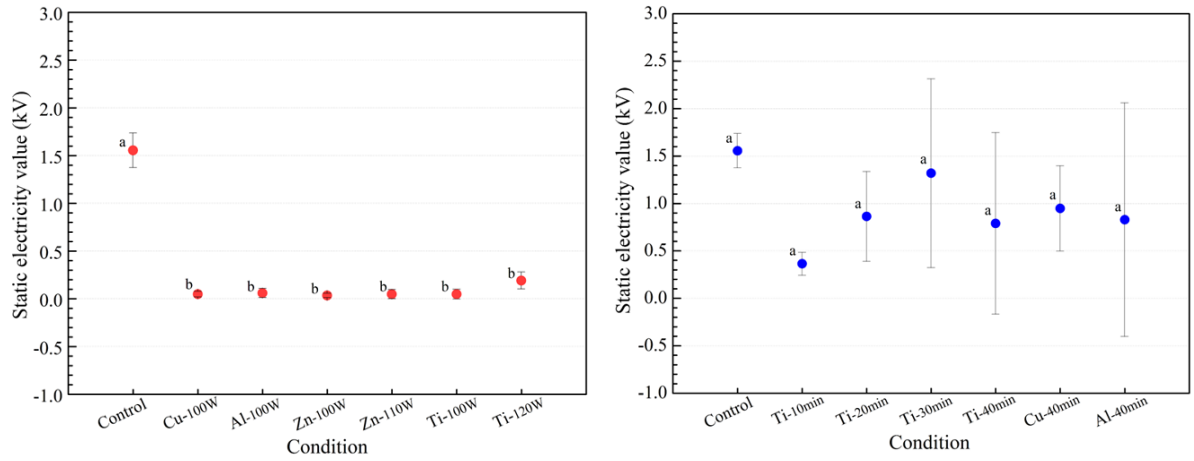

Figure 19. The anti-static behavior of the PBS/E1/PBAT/MgO nanocomposite coated with a magnetron plasma sputtering (left) and sparking (right)

Table 8. The anti-static property of the PBS/E1/PBAT/MgO composite coated nano-metal particle by plasma sputtering and sparking.

Plasma Sputtering		Sparking	
Condition	**Static electricity (kV)**	**Condition**	**Static electricity (kV)**
Control	1.56±0.18[a]	Control	1.56±0.18[a]
Cu-100W	0.05±0.03[b]	Ti-10min	0.36±0.12[a]
Al-100W	0.06±0.05[b]	Ti-20min	0.86±0.47[a]
Zn-100W	0.04±0.02[b]	Ti-30min	1.32±0.99[a]
Zn-110W	0.05±0.05[b]	Ti-40min	0.79±0.96[a]
Ti-100W	0.05±0.05[b]	Cu-40min	0.95±0.45[a]
Ti-120W	0.19±0.09[b]	Al-40min	0.83±1.23[a]

4.2.2 Biodegradability characterization of PBS/E1/PBAT/MgO composite film.

All samples were dried overnight in an oven at 40 °C to remove moisture and obtain accurate weights. Table 9 shows the record of changes in samples' morphology and weight over time for 30 days.

Table 9. Changes in sample morphology and weight over time

No.	Sample	Weight (g)					
		0	**1 day**	**2 days**	**3 days**	**4 days**	**7 days**
1	PBS	 1.05	 1.068	 1.067	 1.066	 1.066	 1.066
2	PBAT	 1.146	 1.159	 1.161	 1.163	 1.162	 1.165
3	PBS/PBAT	 0.902	 0.914	 0.918	 0.916	 0.919	 0.923
4	PBS/E1/PBAT	 1.018	 1.032	 1.035	 1.036	 1.035	 1.035
5	PBS/E1/PBAT/MgO 15	 1.073	 1.096	 1.102	 1.103	 1.098	 1.095

No.	Sample	Weight (g)					
		8 days	10 days	11 days	14 days	16 days	18 days
1	PBS	 1.068	 1.069	 1.071	 1.067	 1.136	 1.144
2	PBAT	 1.169	 1.167	 1.171	 1.169	 1.236	 1.252
3	PBS/PBAT	 0.923	 0.920	 0.925	 0.920	 0.972	 0.981
4	PBS/E1/PBAT	 1.038	 1.036	 1.040	 1.043	 1.104	 1.109
5	PBS/E1/PBAT/MgO 15	 1.095	 1.094	 1.095	 1.092	 1.154	 1.137

No.	Sample	Weight (g)					
		21 days	23 days	25 days	28 days	30 days	-
1	PBS	 1.073	 1.079	 1.078	 1.078	 1.079	-
2	PBAT	 1.172	 1.172	 1.172	 1.174	 1.182	-
3	PBS/PBAT	 0.923	 0.926	 0.925	 0.926	 0.930	-
4	PBS/E1/PBAT	 1.042	 1.040	 1.040	 1.039	 1.043	-
5	PBS/E1/PBAT/MgO 15	 1.060	 1.054	 1.050	 1.050	 1.059	-

In a solid waste environment with a 55% moisture content, moisture is gradually absorbed by the initial weight of a completely dried sample, demonstrating a tendency to increase in weight over a certain period of time. 20 days after the experiment, fine cracks were observed in samples 3 and 5, and sample 3 was completely separated into two pieces on the 25th day (Table 8).

Table 10. The degree of disintegration of test materials.

No.	Sample	m_i (g)	m_{r-1} (g)	m_{r-2} (g)	D (%)
1	PBS	1.050	1.079	1.047	5.3
2	PBAT	1.146	1.182	1.147	4.9
3	PBS/PBAT	0.902	0.930	0.902	5.0
4	PBS/E1/PBAT	1.018	1.043	1.012	5.6
5	PBS/E1/PBAT/MgO 15	1.073	1.059	1.027	9.1

The test materials recovered from the sieving procedure are considered to be non-disintegrated materials. The materials which pass through the sieves are considered to have disintegrated. The degree of disintegration, D, is calculated in % using Formula (2).

$$D = \frac{mi - mr}{mi} X\ 100 \quad (2)$$

where

m_i is the initial dry mass of the test material.

m_{r-1} is the mass of the residual test material after 30 days.

m_{r-2} is the calculated dry mass of the residual test material after 30 days.

Currently, it is not possible to dry the test materials and measure their weight as it is an intermediate stage of the experiment. Therefore, the moisture content due to moisture absorption of the test material was considered to be about 5% and calculated as m_{r-2}. The degree of disintegration was approximately calculated according to m_{r-2}. After the minimum required test period of 45 days has elapsed, the test material will be completely dried to calculate the exact D value.

5. CONCLUSIONS

The successful development of anti-flaming biodegradable composite films marks a significant advancement achieved through the meticulous melt blending of PBS/PBAT and epoxy with MgO. This endeavor has yielded substantial improvements in flame retardancy and mechanical properties, underscoring the potential of these materials for various applications. The incorporation of MgO into the PBS/E1/PBAT blends has not only enhanced thermal decomposition behavior and water resistance but has also fostered improved compatibility among the components. This synergy has led to superior mechanical, water resistance, and thermal properties compared to traditional PBS/PBAT blends.

Moreover, the utilization of the plasma sputter technique for coating the PBS/E1/PBAT/MgO composite with metal or metal oxide has unveiled exceptional anti-static properties, surpassing conventional spark methods. The magnetron sputter deposition technique has emerged as a pivotal tool, offering precise control over nanolayer film thickness, rapid deposition rates, exceptional adhesion, high purity, and stability.

Furthermore, the examination of the composite films in a simulated solid waste environment with 55% moisture content has provided valuable insights into their potential degradation behavior. The gradual absorption of moisture by the dried samples has led to observable changes over time, such as weight increase and the emergence of fine cracks, shedding light on their environmental response and durability.

In summary, these findings collectively underscore the promising applicability of the developed anti-flaming biodegradable composite films, particularly in sectors such as packaging, medical, and agriculture. The exploration of advanced coating techniques like plasma sputtering opens avenues for further enhancement and innovation in sustainable materials research, paving the way for greener and more resilient solutions in diverse industries.

6. REFERENCES

Al Ghufais, I. A., Rahaman, M., & Aldalbahi, A. Evaluation of Physical Properties of Recycled Polyethylene Waste Films and Application of its Carbon filled Composites as Anti-static Material in Electronic Packaging.

Battegazzore, D., Frache, A., & Carosio, F. (2020). Layer-by-Layer nanostructured interphase produces mechanically strong and flame retardant bio-composites. Composites Part B: Engineering, 200, 108310.

Bumbudsanpharoke, N., Wongphan, P., Promhuad, K., Leelaphiwat, P., & Harnkarnsujarit, N. (2022). Morphology and permeability of bio-based poly(butylene adipate-co-terephthalate) (PBAT), poly(butylene succinate) (PBS) and linear low-density polyethylene (LLDPE) blend films control the shelf-life of packaged bread. Food Control, 132, 108541. https://doi.org/https://doi.org/10.1016/j.foodcont.2021.108541

Can-Herrera, L., Ávila-Ortega, A., de la Rosa-García, S., Oliva, A., Cauich-Rodríguez, J., & Cervantes-Uc, J. (2016). Surface modification of electrospun polycaprolactone microfibers by air plasma treatment: Effect of plasma power and treatment time. European Polymer Journal, 84, 502-513.

de Matos Costa, A. R., Crocitti, A., Hecker de Carvalho, L., Carroccio, S. C., Cerruti, P., & Santagata, G. (2020). Properties of Biodegradable Films Based on Poly(butylene Succinate) (PBS) and Poly(butylene Adipate-co-Terephthalate) (PBAT) Blends. Polymers, 12(10), 2317. https://www.mdpi.com/2073-4360/12/10/2317

Deng, Y., Yu, C., Wongwiwattana, P., & Thomas, N. L. (2018). Optimizing Ductility of Poly(Lactic Acid)/Poly(Butylene Adipate-co-Terephthalate) Blends Through Co-continuous Phase Morphology. Journal of Polymers and the Environment, 26(9), 3802-3816. https://doi.org/10.1007/s10924-018-1256-x

Dhanumalayan, E., Trimukhe, A. M., Deshmukh, R. R., & Joshi, G. M. (2017). The disparity in hydrophobic to hydrophilic nature of polymer blend modified by K2Ti6O13 as a function of air plasma treatment. Progress in Organic Coatings, 111, 371-380. https://doi.org/https://doi.org/10.1016/j.porgcoat.2017.06.001

European bioplastics. (2021). Bioplastics market data. Retrieved 21/04/2022 from https://www.european-bioplastics.org/market/

Feng, J., Sun, Y., Song, P., Lei, W., Wu, Q., Liu, L., Yu, Y., & Wang, H. (2017). Fire-resistant, strong, and green polymer nanocomposites based on poly (lactic acid) and core-shellnanofibrous flame retardants. ACS Sustainable Chemistry & Engineering, 5(9), 7894-7904.

Formela, K., Zedler, Ł., Hejna, A., & Tercjak, A. (2018). Reactive extrusion of bio-based polymer blends and composites – Current trends and future developments. eXPRESS Polymer Letters, 12, 24-57. https://doi.org/10.3144/expresspolymlett.2018.4

Jiang, D., Pan, M., Cai, X., & Zhao, Y. (2018). Flame retardancy of rice straw-polyethylene composites affected by in situ polymerization of ammonium polyphosphate/silica. Composites Part A: Applied Science and Manufacturing, 109, 1-9.

Lee, K. (2018). What Are the Effects of Non-Biodegradable Waste? sciencing. Retrieved 21/04/2022 from https://sciencing.com/styrofoam-biodegradable-22340.html

Li, H., Ning, N., Zhang, L., Wang, Y., Liang, W., & Tian, M. (2014). Different flame retardancy effects and mechanisms of aluminium phosphinate in PPO, TPU and PP. Polymer Degradation and Stability, 105, 86-95. https://doi.org/https://doi.org/10.1016/j.polymdegradstab.2014.03.032

Liminana, P., Garcia-Sanoguera, D., Quiles-Carrillo, L., Balart, R., & Montanes, N. (2018). Development and characterization of environmentally friendly composites from poly(butylene succinate) (PBS) and almond shell flour with different compatibilizers. Composites Part B: Engineering, 144, 153-162. https://doi.org/https://doi.org/10.1016/j.compositesb.2018.02.031

Lule, Z. C., Wondu, E., & Kim, J. (2021). Highly rigid, fire-resistant, and sustainable polybutylene adipate terephthalate/polybutylene succinate composites reinforced with surface-treated coffee husks. Journal of Cleaner Production, 315, 128095. https://doi.org/https://doi.org/10.1016/j.jclepro.2021.128095

Nobile, M. R., Crocitti, A., Malinconico, M., Santagata, G., & Cerruti, P. (2018). Preparation and characterization of polybutylene succinate (PBS) and polybutylene adipate-terephthalate (PBAT) biodegradable blends. AIP Conference Proceedings,

OECD. (2022). Plastic pollution is growing relentlessly as waste management and recycling fall short, says OECD. OECD. Retrieved 21/04/2022 from https://www.oecd.org/environment/plastic-pollution-is-growing-relentlessly-as-waste-management-and-recycling-fall-short.htm

Qin, Z., Yang, R., Zhang, W., Li, D., & Jiao, Q. (2019). The synergisticbarrier effect of aluminum phosphate on flame retardant polypropylene based on ammonium polyphosphate/dipentaerythritol system. Materials & Design, 181, 107913. https://doi.org/10.1016/j.matdes.2019.107913

Rafiqah, S. A., Khalina, A., Harmaen, A. S., Tawakkal, I. A., Zaman, K., Asim, M., Nurrazi, M. N., & Lee, C. H. (2021). A Review on Properties and Application of Bio-Based Poly(Butylene Succinate). Polymers, 13(9), 1436. https://www.mdpi.com/2073-4360/13/9/1436

Rodrigues, B. V., Silva, A. S., Melo, G. F., Vasconscellos, L. M., Marciano, F. R., & Lobo, A. O. (2016). Influence of low contents of superhydrophilic MWCNT on the properties and cell viability of electrospun poly (butylene adipate-co-terephthalate) fibers. Materials Science and Engineering: C, 59, 782-791.

Silva, T. F. d., Menezes, F., Montagna, L. S., Lemes, A. P., & Passador, F. R. (2019). Preparation and characterization of antistatic packaging for electronic components based on poly (lactic acid)/carbon black composites. Journal of Applied Polymer Science, 136(13), 47273.

Stöckel, S., Ebert, S., Böttcher, M., Seifert, A., Wamser, T., Krenkel, W., Schulze, S., Hietschold, M., Gnaegi, H., & Goedel, W. A. (2014). Coating of Alumina Fibres With Aluminium Phosphate by a Continuous Chemical Vapour Deposition Process. Chemical Vapor Deposition, 20(10-11-12), 388-398. https://doi.org/https://doi.org/10.1002/cvde.201407099

Turkoglu Sasmazel, H., Alazzawi, M., & Kadim Abid Alsahib, N. (2021). Atmospheric Pressure Plasma Surface Treatment of Polymers and Influence on Cell Cultivation. Molecules, 26(6), 1665. https://www.mdpi.com/1420-3049/26/6/1665

Xu, J., & Guo, B. H. (2010). Poly (butylene succinate) and its copolymers: Research, development and industrialization. Biotechnology journal, 5(11), 1149-1163.

Zoubek, M., Kudláček, J., Kreibich, V., Jirout, T., & Abramov, A. (2019). The Influence of Mixing Method and Mixing Parameters in Process of Preparation of Anti-static Coating Materials Containing Nanoparticles. In B. Gapiński, M. Szostak, & V. Ivanov, Advances in Manufacturing II Cham.

Abbreviation

PBS	Polybutylene succinate
PBAT	Polybutylene adipate terephthalate
MgO	Magnesium oxide
ABS	Acrylonitrile butadiene styrene
UL94	Plastics flammability standard released by the Underwriters Laboratories (USA)
NMP	Nano metal particles
E1	1% of epoxy blended with polymer composite.
PBS/PBAT	Polybutylene succinate blended with Polybutylene adipate terephthalate.
PBS/E1/PBAT	Polybutylene succinate blended with polybutylene adipate terephthalate and 1% of epoxy
T1, T2	T1: Time after first flame applications T2: Time after second flame applications
V0, V1, V2	Vertical Burning Test V0: if the flame extinguishes within 10 seconds with no dripping V1: if the flame extinguishes within 30 seconds with no dripping V2: if the flame extinguishes within 10 seconds with dripping